Copyright

by

Kristin Victoria Grubbs

1997

The Effect of the Dogbone Connection on the Elastic Stiffness of Steel Moment Frames

by

Kristin Victoria Grubbs, B.S.

Thesis

Presented to the Faculty of the Graduate School of

The University of Texas at Austin

in Partial Fulfillment

of the Requirements

for the Degree of

Master of Science in Engineering

The University of Texas at Austin

August 1997

The Effect of the Dogbone Connection on the Elastic Stiffness of Steel Moment Frames

Approved by
Supervising Committee:

_____

_____

Acknowledgements

The author wishes to express her appreciation and gratitude to her supervisor, Dr. Michael D. Engelhardt, for his guidance and support throughout the research, and writing of this thesis. The author also wishes to express his deep gratitude to Dr. Joseph A. Yura for his assistance on this thesis. The author also wants to thank her family for all the love and support that was given throughout this time. Special thanks are also extended to Chris Gilchrist for his guidance and encouragement. Finally, the author is grateful to all her friends, fellow students, and roommates who provided love, support, advice, and assistance.

July 14, 1997

Abstract

The Effect of the Dogbone Connection on the Elastic Stiffness of Steel Moment Frames

Kristin Victoria Grubbs, M.S.E.

The University of Texas at Austin, 1997

Supervisor: Michael D. Engelhardt

Developed after the 1994 Northridge Earthquake, the radius-cut reduced beam section, or the "dogbone" connection, has proved to be a promising alternative for steel moment frame connections. Although a favored alternative, some potentially important aspects of the dogbone connection have not been completed. The effect of the dogbone cutout on the elastic lateral stiffness of a frame is one of these concepts. The three objectives of this report are: to analyze the reduction in stiffness of an individual cantilever beam, to develop a simplified analysis using frame elements, and to analyze the reduction in stiffness of an overall frame. The information contained in this report will be useful in determining whether to continue to ignore the effects of the cutout on stiffness or rather to design taking the reduced stiffness into account.

Table of Contents

List of Tables vii

List of Figures viii

Chapter 1 Introduction 1

The Development of the RBS Connection 1

Testing on Reduis-Cut Dogbones 3

Objectives of Research 4

Chapter 2 Finite Element Analysis of Cantilever Beams 7

The Finite Element Models 7

Results 15

Verification of Results 16

Chapter 3 Simplified Analysis Using Frame Elements 19

Overview of Analysis Approach 21

Results 25

Comparsion with Finite Element Results 31

Chapter 4 Frame Analysis 33

The Frame Models 33

Results 41

Chapter 5 Summary and Design Recommendations 50

Summary 50

Design Recommendations 52

Bibliography 53

Vita 55

List of Tables

Table 2.1: Dimensions of Models 10

Table 2.2: Average Displacements (inches) 15

Table 2.3: Comparison of Tip Displacements: Finite Element Solution vs. Simplified Closed Form Solution 18

Table 3.1: Results for Dogbones with 40 Percent Cutouts 25

Table 3.2: I_r/I for Various Cutouts (%) 27

Table 3.3: I_r/I for Various Cutouts (%) - Dogbone Length Increased by 50 Percent 28

Table 3.4: Summary of Results 29

Table 3.5: Comparison of Tip Displacements: Simplified Analysis Using Frame Elements vs. Finite Element Analysis 32

Table 4.1: Results of Frame 1 Analysis 43

Table 4.2: Results of Frame 2 Analysis 43

Table 4.3: Results of Frame 3 Analysis 44

Table 4.4: Results of Frame 4 Analysis 44

Table 4.5: Change in Stiffness Resulting From Dogbone - Frame 1 46

Table 4.6: Change in Stiffness Resulting From Dogbone - Frame 2 46

Table 4.7: Change in Stiffness Resulting From Dogbone - Frame 3 47

Table 4.8: Change in Stiffness Resulting From Dogbone - Frame 4 47

List of Figures

Figure 1.1: Typical Dogbone Cutouts 2

Figure 2.1: Beam Cross Sections 8

Figure 2.2: Key Dimensions of the Cutout 9

Figure 2.3: The Finite Element Model Meshes of W36X150 12

Figure 2.4: The Finite Element Model Meshes of W30X148 13

Figure 2.5: The Finite Element Model Meshes of W24X68 14

Figure 3.1: Simplified Analysis Using Frame Elements 20

Figure 3.2: M/EI Diagram for Beam Using the Exact I 22

Figure 3.3: M/EI Diagram for Beam with I_e 24

Figure 3.4: Plot of I_e/I vs. Flange Cutout 30

Figure 4.1: Frame 1 34

Figure 4.2: Frame 2 35

Figure 4.3: Frame 3 36

Figure 4.4: Frame 4 37

Figure 4.5: Rigid End Offsets (Wilson & Habibullah, 1990) 39

Figure 4.6: The Frame Model Dimensions 40

Figure 4.7: Two Loading Cases 41

Chapter 1: Introduction

During the 1994 Northridge Earthquake, failures of welded beam-column connections in steel moment resisting frames were prevalent. From this discovery, a number of improved steel moment connections have been proposed (SAC, August, 1995). In general, the overall goal in the development of new connections is to provide ductility in the seismic response, to provide a reliable performance, and to render an economical solution. Many of the new connections developed since the Northridge Earthquake have been reinforced with cover plates, ribs, haunches, side plates, or other devices. An alternative to reinforced connections, the reduced beam section (RBS) or the "dogbone" connection, has proved to be a promising alternative for steel moment frames.

The Development of the RBS Connection

From plastic theory, when a member has become fully plastic due to a bending moment, any attempt to increase the moment causes the member to act like a plastic hinge. With a plastic hinge present, large rotations are possible without any significant changes in the resisting moment (Horne & Morris, 1981). The large rotations signify high ductility in the member. In a strong earthquake, plastic hinges are intended to form at the beam ends in a steel moment frame. When the connection is reinforced, the plastic hinges are forced away from the face of the column which reduces the stress at the connection. By selectively trimming the flanges of the beams, the stresses tend to develop at these weaker zones, therefore moving the stresses away from the beam-column connection and

still allowing large rotations at the plastic hinges. These reduced sections of the beam allow the connection strength to exceed the beam strength without the need for reinforcing the connection. By moving the stresses away from the beam-to-column connection, yielding occurs in the reduced section and the potential for brittle failure at the connection is reduced.

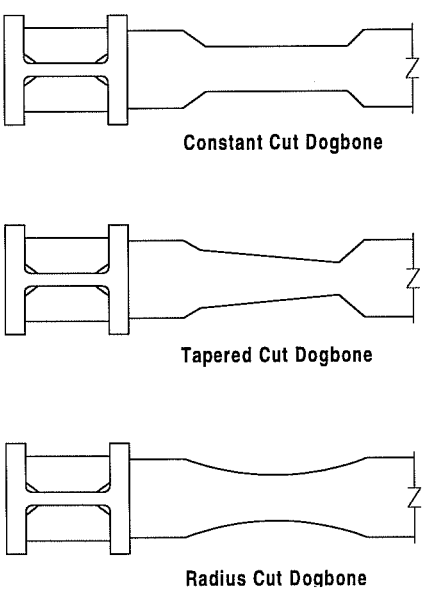

Figure 1.1: Typical Dogbone Cutouts

Dogbone type connections have been proposed and tested by a number of investigators. Various shape cutouts, as shown in Figure 1.1, have been investigated. Rea, Clough, and Bouwkamp (1969) employed a constant cut dogbone at a column base connection. Plumier (1990) appears to have examined both constant and tapered cut dogbones. Chen and Yeh (1994) conducted a series

of five tests on tapered cut dogbones. All of these investigations preceded the Northridge Earthquake and demonstrated the potential improvement in performance possible with dogbone cutouts in the beam.

After the Northridge Earthquake, testing of dogbone connections was continued with renewed interest. Iwankiw and Carter (1996) tested four large scale specimens constructed with tapered cut dogbones. These specimens developed large levels of ductility, although two of the four ultimately developed fractures at the beam-to-column connections. Zekioglu, et. al, (1997) tested five large scale specimens with tapered cut dogbones. In addition to the dogbone cutouts in the beam, the connection was further reinforced with ribs. These specimens also developed large levels of ductility, but ultimately failed by fracture of the beam within the dogbone region. The fractures developed at the minimum section of the tapered cut, apparently due to a stress concentration at the change in cross-sectional area.

More recently, tests have been conducted on radius-cut dogbones shown in Figure 1.1 (Engelhardt, et.al., 1996). The radius cut minimizes stress concentrations within the dogbone region, and has shown excellent performance in laboratory testing, as described below.

Testing on Radius-Cut Dogbones

A test program conducted at The University of Texas at Austin (Engelhardt, et. al., 1996) consisted of four large-scale specimens with radius-cut dogbones. In addition to the dogbone cutouts in the beam, welding and design

improvements were incorporated into the beam-to-column connection to improve the capabilities of the connection.

Each of the four specimens showed excellent performance with plastic rotations exceeding 0.03 radians for each specimen, indicating high ductility. At the point at which testing was stopped, no fractures had developed within the dogbone region for any of the radius-cut specimens, and no failures occurred at the beam-to-column connection. Testing was stopped because of testing equipment limitations, rather than the failure of the specimen. Additional successful tests of radius-cut dogbones have been conducted by Popov (1996) and by Tremblay, et. al. (1997).

Overall, the radius-cut dogbone has proved in testing to be highly ductile and reliable. In cost comparisons completed by W&W Steel (Oklahoma City), the radius-cut dogbone connection also proved to be one of the most economical alternatives among a number of improved moment connection details (Engelhardt, et. al, 1996). The successful testing combined with the favorable economics of the radius-cut dogbone connection make it one of the most promising options for moment resisting beam-to-column connections. Although a promising alternative, a few aspects of the dogbone connections have not been completely investigated, as discussed in the next section.

Objectives of Research

Although considerable research and testing have been completed, some potentially important aspects of the radius-cut dogbone connection have not been investigated. One of these aspects is the effect of the dogbone cutout on the

elastic stiffness of the frame. Previous researchers (Plumier 1990, Chen-Yeh 1994, Engelhardt, et.al 1996) have suggested that the reduction in elastic stiffness is likely to be small. In tests on tapered cut dogbones, Chen-Yeh (1994) measured a three percent reduction in stiffness resulting from the addition of the dogbone cutouts. Overall, however, very little research appears to have been done in the past to accurately quantify the reduction in frame-lateral stiffness that results from dogbone cutouts in the beams.

Beam sizes in steel moment frames are frequently controlled by code drift limitations rather than by code strength requirements. Consequently, a reduction in stiffness due to the use of dogbones could potentially results in the need for increased member sizes. Accurately quantifying the effect of dogbones on stiffness is therefore an important issue in the design process. This report will examine the change in frame elastic stiffness that results from the use of radius-cut dogbones.

The first objective of this report was to analyze the reduction of stiffness of an individual cantilever beam. By using finite element analysis, several cantilever beams of varying size and length were modeled with and without the radius-cut dogbone connection. The purpose was to examine the stiffness of the beams with and without the cutout, and to determine if altering the span length has any effect on the reduction in stiffness.

The next objective was to derive an effective moment of inertia for the reduced section to permit simplified analysis of beams with radius-cut dogbones. By using the moment-area method, an effective moment of inertia was derived. Analysis of several beam sizes with various flange cutout widths were performed.

A separate member with this reduced moment of inertia can be used for the cutout region in a frame analysis program.

The final objective of this report was to analyze the effect of the dogbone connection on the stiffness of an entire frame. By using the previously derived effective moment of inertia, the frames were modeled with and without the dogbone cutout. A variety of steel moment frames were analyzed using several different sizes of dogbone cutouts.

Chapter 2: Finite Element Analysis of Cantilever Beams

The first step in analyzing the effect of the dogbone connection on the elastic stiffness of a frame was to consider the change in stiffness of isolated cantilever beams with and without the radius-cut dogbone connection. The stiffness was examined by observing the changes in displacement obtained by a finite element analysis. The finite element computer program used was SAP90.

SAP90 is a widely used commercial elastic structural analysis computer program (Wilson & Habibullah, 1989). SAP90 performs static and dynamic analysis, and is designed to run on personal computers. The element library consists of basically four types of elements: frame, shell, asolid, and solid elements. Model generation options are available for convenience and plotting capabilities are available to check model geometry. During analysis, the stiffness method is used to solve for joint displacements, reactions, forces, and stresses.

The Finite Element Models

The three following structural steel shapes were modeled using SAP90: W36X150, W30X148, and W24X68. Twelve different cantilever beams were analyzed. The three different size beams were each modeled for two cases: with and without the radius-cut dogbone connection. Each case was then modeled with a 15 foot cantilever and a 20 foot cantilever. As shown in Figure 2.1, the modeled cross sections differ slightly from the standard rolled structural shapes. The basic dimensions are the same, but the beams were modeled with sharp corners instead of filleted corners between the flanges and the web.

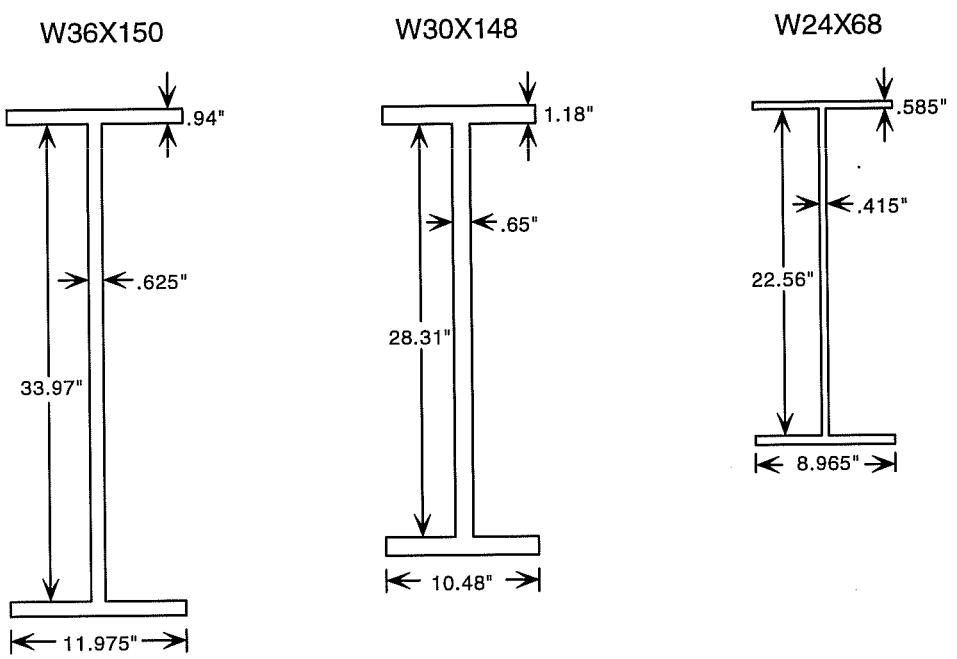

Figure 2.1: Beam Cross Sections

The cantilever beams were fixed on one end and a concentrated load was placed at the tip. This concentrated load was distributed along the height of the web. The length of the beam was representative of half of an actual moment frame bay, assuming a point of inflection at mid-span. The 15 foot cantilever therefore modeled a 30 foot clear span beam, and the 20 foot cantilever modeled a 40 foot clear span beam. The cantilever tip displacements were compared with and without the dogbone in order to evaluate the change in stiffness of the beam. The goal of the finite element analysis was not only to examine the effects of the

radius-cut dogbone connection on stiffness, but also to determine if the change in stiffness was dependent on beam sizes and span lengths.

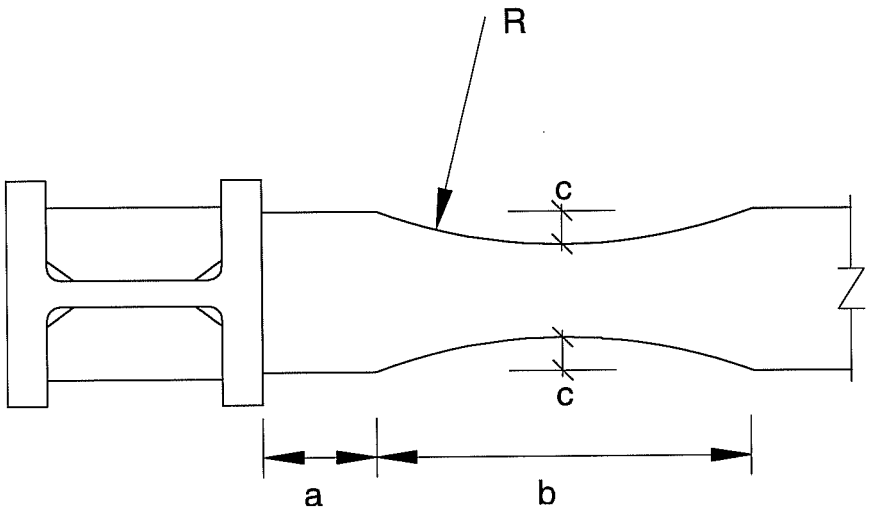

Figure 2.2: Key Dimensions of the Cutout

When designing the beams with the radius-cut dogbone connection, dimensions of the dogbone were very important. The dimensions of a typical radius-cut dogbone were suggested by the authors of the article, "The Dogbone Connection: Part II," *Modern Steel Construction*, August 1996 (Engelhardt, et. al, 1996). Figure 2.2 shows these key dimensions. Values for the cutout dimensions were recommended based on testing of the radius-cut dogbone and experience with other connection test programs. The distance "a" is measured from the face of the column to the start of the dogbone. Values for the distance "a" were suggested in the range of 50 to 75 percent of the beam flange width. The length of the cut, "b", was suggested to be approximately 65 to 85 percent of the beam depth. The dimensions "a" and "b" should be kept small in order to minimize the

amplification of moment from the hinge location in the dogbone to the face of the column. The dimensions must also be large enough to allow the stresses in the reduced beam flange to spread uniformly over the flange width and to avoid excessive inelastic strains in the dogbone.

The crucial dimension is the depth of the cut, "c". This depth was chosen to limit the maximum moment at the face of the column to values in the range of about 85 to 100 percent of the plastic moment of the beam. This depth of the cut removed approximately 40 percent of the beam flange width (Engelhardt, et. al, 1996). Based on the equation of a circle, the radius, "R", of the cut is computed by the formula:

$$R = \frac{4c^2 + b^2}{8c} \tag{2.1}$$

The actual dimensions of the cutouts for the various beam sizes modeled are shown in Table 2.1. In each case, approximately 40 percent of the beam flange width was removed at the minimum section of the dogbone.

Table 2.1: Dimensions of Models

	a	b	c	R
W36X150	9″	27″	2.375″	39.556″
W30X148	5″	25″	2″	40.0625″
W24X68	5″	16″	1.75″	19.161″

The cantilever beams were modeled by using the eight-noded solid element or "brick" element. Several trial models were run using different

numbers of elements in order to achieve accurate results. Each beam was modeled without the dogbone with approximately 1000, 2500, and 4000 nodes. The displacements of each model were compared with displacements found from the closed form solution which is discussed later in this chapter. By using as many nodes as possible (SAP90 permits a maximum of 4000 nodes), it was found that the model provided accurate predictions of displacement with an error of less than 0.5 percent. Thus, each beam consisted of approximately 4000 nodes and 1800 elements. As shown in Figure 2.3, 2.4, and 2.5, the meshes of the models with the dogbones differed slightly. In all of the beams, the nodes were spaced closer together in and around the cutout region and then increased in spacing as the distance from the cutout region increased. As a result of the different dimensions of the cutout among the different beam sizes, the nodal spacing along the length of the member varied slightly. To accommodate the changing span lengths, the nodal spacing along the length was altered for the same size beam. In each model, the flange of the beam was broken up into three elements across its width with the middle element being the width of the web. The web consisted of ten elements along its height in between the flanges.

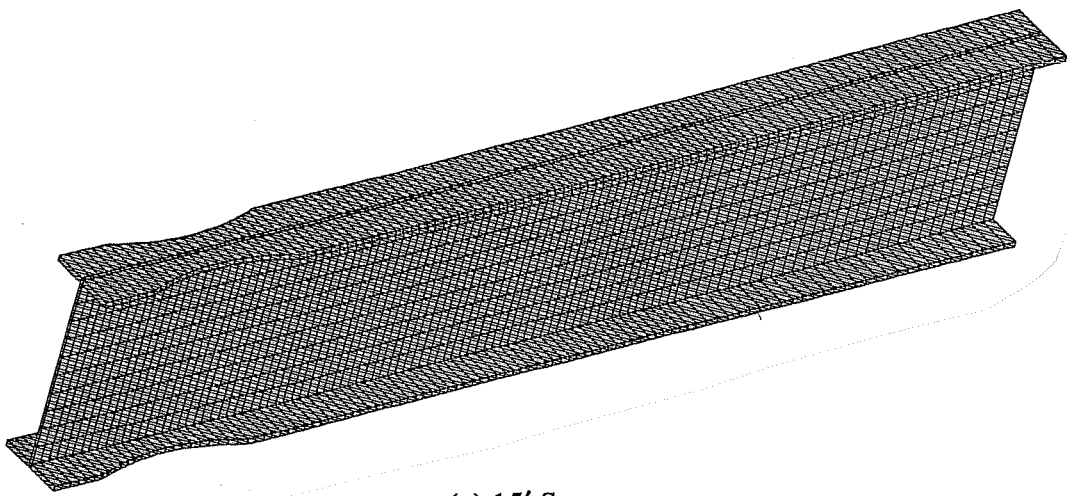

(a) 15′ Span

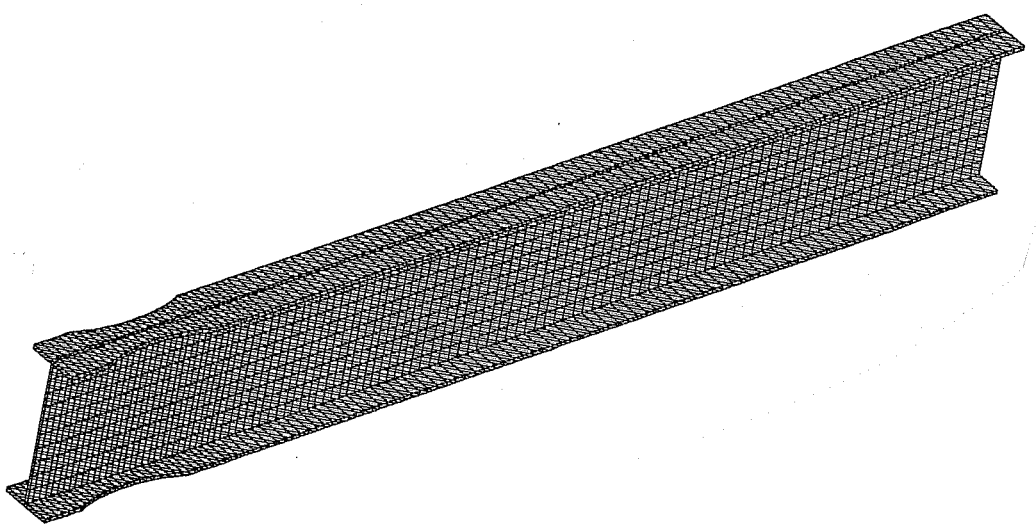

(b) 20′ Span

Figure 2.3: The Finite Element Model Meshes of W36X150

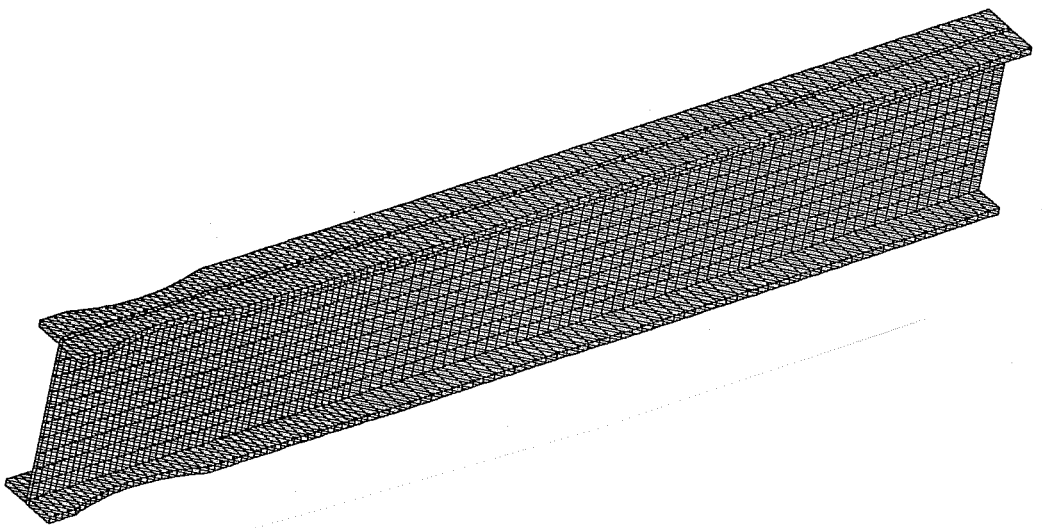

(a) 15′ Span

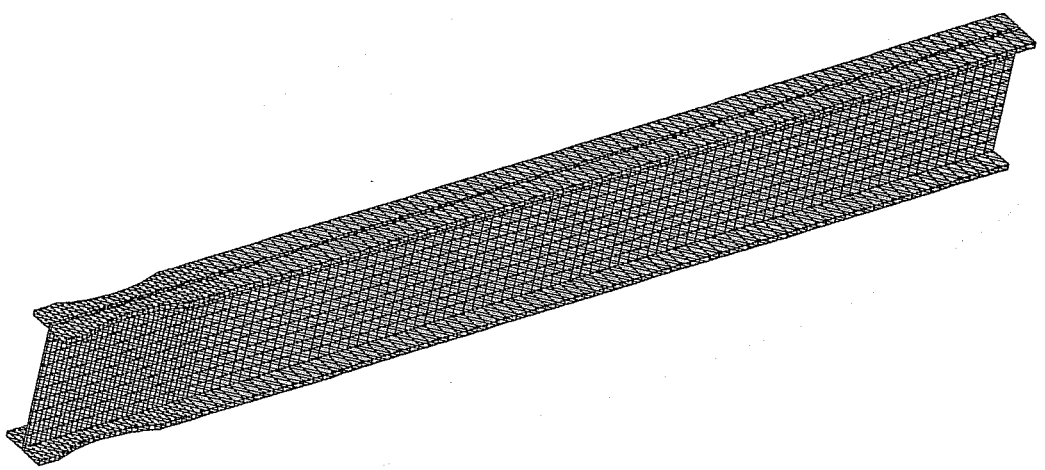

(b) 20′ Span

Figure 2.4: The Finite Element Model Meshes for W30X148

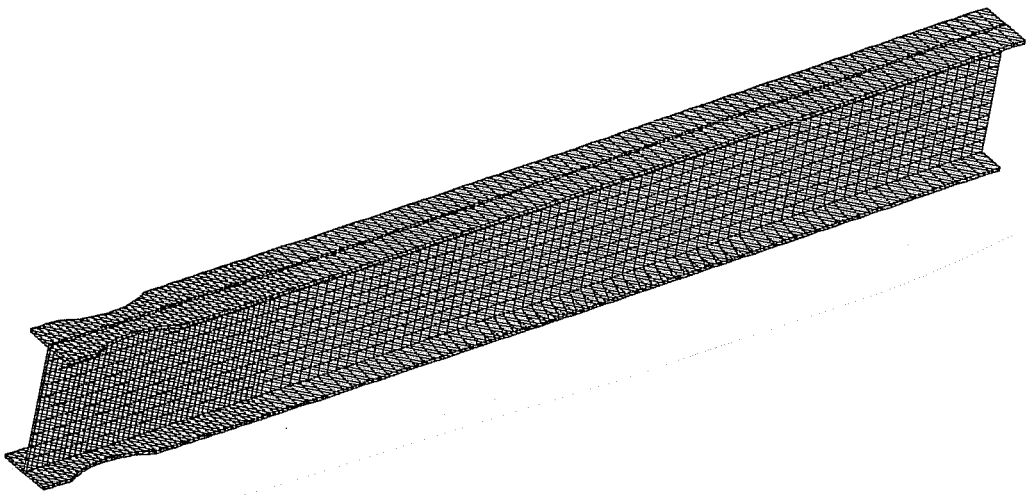

(a) 15′ Span

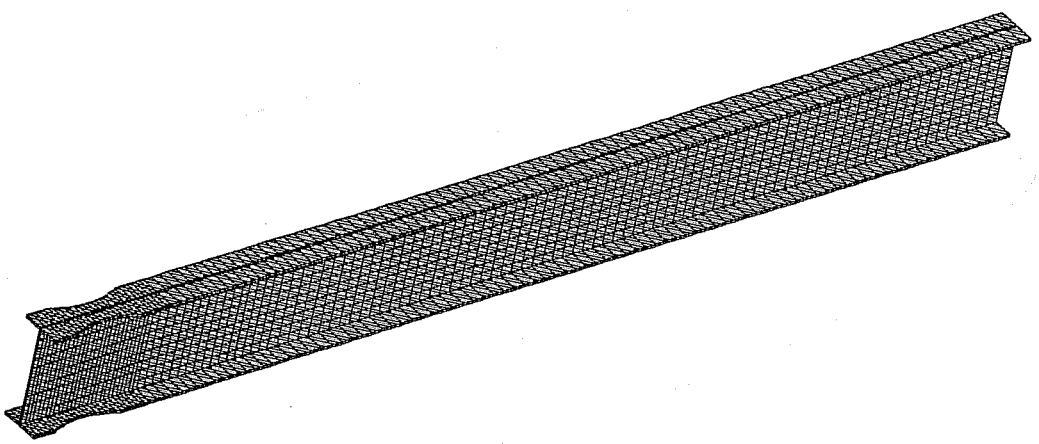

(b) 20′ Span

Figure 2.5: The Finite Element Model Meshes for W24X68

Results

A 260 kip load was distributed across the web at the tip of each beam. The tip displacements for the nodes across the base of the bottom flange were then averaged. The average tip displacement of the each beam is shown in Table 2.2.

Table 2.2: Average Displacements (inches)

	Displacements		Percent Reduction in Stiffness
	Without Dogbone (in)	With Dogbone (in)	
W36X150			
15′ Span	2.076	2.274	8.7
20′ Span	4.763	5.140	7.3
W30X148			
15′ Span	2.753	3.016	8.7
20′ Span	6.309	6.801	7.2
W24X68			
15′ Span	9.754	10.427	6.5
20′ Span	22.685	23.928	5.2

By taking the average tip displacements of a beam with and without the dogbone, the percent reduction in stiffness of the beam was calculated. The radius-cut dogbone connection resulted in a reduction in stiffness of 5-9 percent for the beams. The larger beams, W36X150 and W30X148, displayed a slightly higher reduction in stiffness than the smaller W24X68 beam. The longer spans tended to show a lower reduction in stiffness than the shorter spans. The reduction in overall frame stiffness due to the dogbone cutouts in the beams will be less than

the values shown in Table 2.2, since the beams are only one component of the frame. This issue will be investigated in Chapter 4.

Verification of Results

In order to evaluate the accuracy of the finite element model, the tip displacement predicted by the finite element model for the cantilever without a dogbone cutout was compared to a simplified closed form solution. The closed form tip displacement was computed as follows:

$$\Delta_b = \frac{PL^3}{3EI}$$

$$\Delta_s = \frac{PL}{A_w G}$$

$$\Delta = \Delta_b + \Delta_s$$

where:

Δ_b = tip displacement due to bending
Δ_s = tip displacement due to shear
Δ = total tip displacement
P = tip load
L = length of cantilever
I = moment of inertia
A_w = web area
E = elastic modulus
G = elastic shear modulus

The results of this simplified closed form solution is shown in Table 2.3, and is compared to the finite element solution. The difference between the two solutions is small, typically less than 0.5 percent. This small difference does not necessarily imply a small error in the finite element model, since the closed form solution is also approximate. In any event, the close agreement between these

solutions suggests that the finite element model is providing accurate estimates of displacement.

Table 2.3: Comparison of Tip Displacements: Finite Element Solution vs. Simplified Closed Form Solution

	Tip Displacement - Closed Form (inches)			Tip Displacement Finite Element (inches)	Percent Difference Between Closed Form & Finite Element
	Displacement Due to Bending	Displacement Due to Shear	Total Displacement		
W36X150					
15′ Span	1.892	0.189	2.081	2.076	0.252
20′ Span	4.486	0.253	4.739	4.763	0.496
W30X148					
15′ Span	2.550	0.220	2.770	2.753	0.593
20′ Span	6.042	0.294	6.336	6.309	0.438
W24X68					
15′ Span	9.349	0.433	9.782	9.754	0.292
20′ Span	22.16	0.578	22.738	22.685	0.234

Chapter 3: Simplified Analysis Using Frame Elements

In Chapter 2, the reduction in elastic stiffness of a cantilever beam resulting from a dogbone cutout was evaluated by finite element analysis. The cantilever beam was discretized into a large number of 3-dimensional solid elements. While this approach can provide accurate results, its usefulness for analyzing entire frames is limited due to the large number of elements required, and the extensive effort required in developing the model. Further, this approach does not lend itself well to routine design office use. Consequently, in this chapter, a simplified approach will be developed for evaluating the change in elastic stiffness resulting from dogbone cutouts in the beams of moment frames subject to lateral loads.

In typical design practice, beams and columns are analyzed using one-dimensional frame elements. In order to use a frame element to model the dogbone region of the beam, the properties of the element must be modified to reflect the changes in cross section. The approach that will be taken in this chapter will be to model the dogbone region with a single prismatic frame element, i.e., a frame element where the cross sectional properties are constant along the length of the element. Since the actual cross section varies continuously along the dogbone, an effective moment of inertia, I_e, must be determined for the prismatic beam element that will adequately reflect the stiffness of the dogbone portion of the beam. The overall approach is illustrated in Figure 3.1. The portions of the beam outside of the dogbones is modeled as

usual, i.e., with frame elements using the member's full moment of inertia, I. The dogbone regions, of length b, are modeled with frame elements using a reduced value of I_e. The goal of this chapter is to develop recommendations for choosing values of I_e for various depths of cuts. These results will then be used in Chapter 4 for analyzing entire frames. This approach can be easily implemented in commercial structural analysis computer programs, and should therefore be useful in routine design office analysis of moment frames with dogbones.

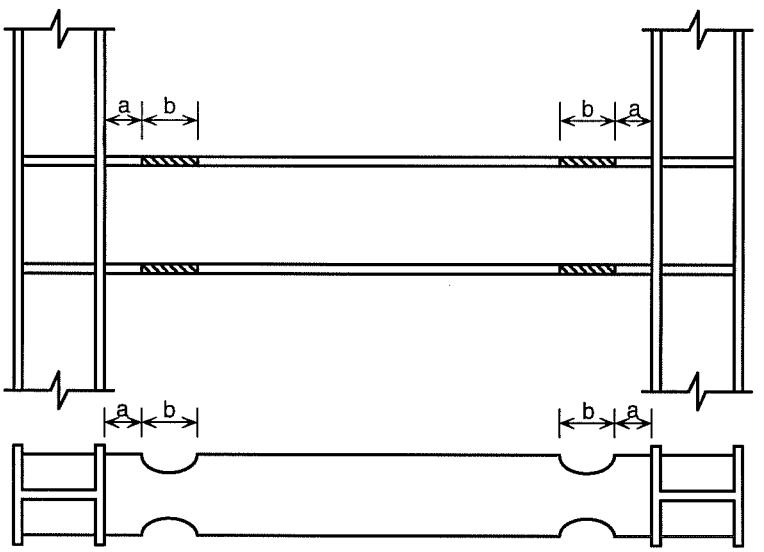

(a) Moment frame beam with dogbone cutouts

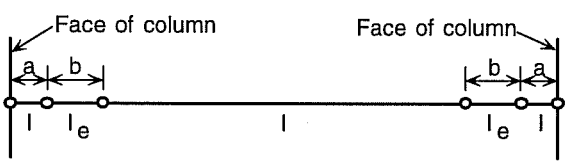

(b) Simplified model of moment frame beam using prismatic frame elements

Figure 3.1: Simplified Analysis Using Frame Elements

In addition to modifying the moment of inertia for the dogbone frame element, the area should also be reduced. However, in the present study, it is assumed that the axial forces in the beams are very low, so that the axial stiffness of the beam has no significant effect on the lateral deflection of the frame. Consequently, no modifications will be made to the cross-sectional area assigned to the dogbone element; only the moment of inertia will be modified.

Overview of Analysis Approach

In order to establish values of I_e, the following approach was taken. A cantilever beam subject to a tip load was analyzed. The tip deflection was computed using the moment-area method. With this method, the tip deflection can simply be computed as the first moment of the area under the M/EI diagram (i.e., the curvature diagram, taken about the tip).

As a first step, tip deflections were computed for cantilever beams with dogbone cutouts using exact values for the moment of inertia. The moment of inertia varies continuously along the length of the dogbone. An expression was developed for the exact values of moment of inertia at any point along the dogbone, and this expression was then used to establish the M/EI diagram. This M/EI diagram is qualitatively illustrated in Figure 3.2. The tip deflection was computed as the first moment of the area under the M/EI diagram taken about the tip, using numerical integration. The M/EI diagram was divided into a number of small strips along the length of the beam. For each strip, the area of the strip was computed using the trapezoidal rule. The area of the strip was then multiplied by

the distance from the center of the strip to the tip of the cantilever. The tip deflection was then obtained by summing all strips.

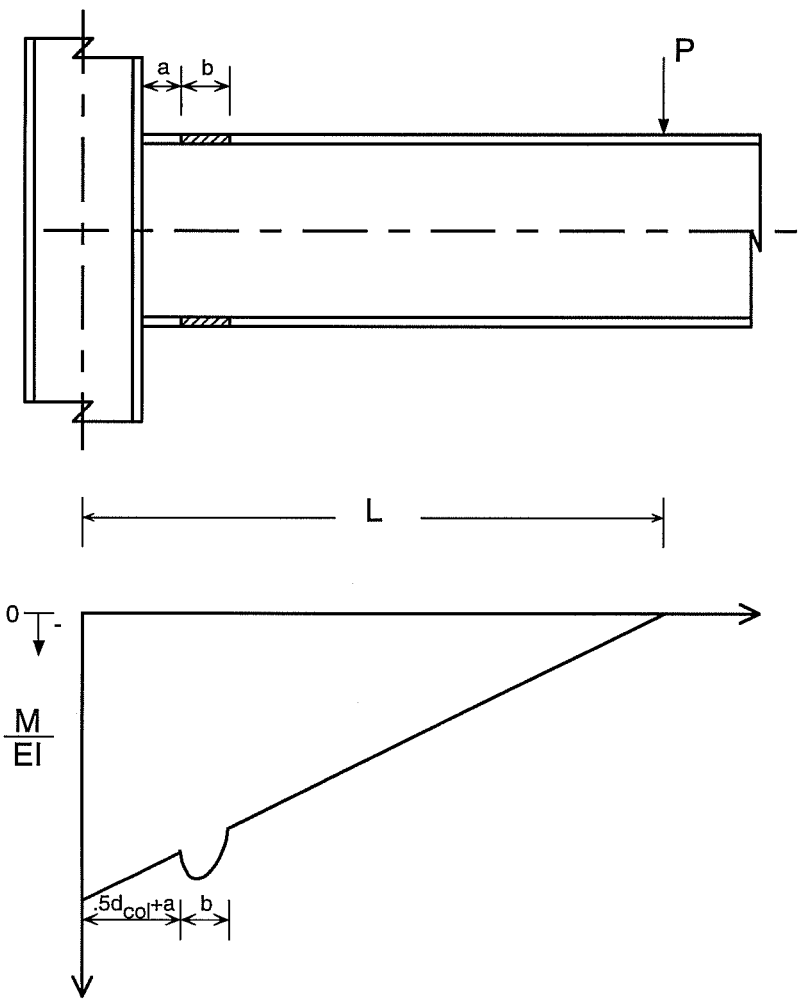

Figure 3.2: M/EI Diagram for Beam Using the Exact *I*

As the next step, the same cantilever was analyzed assuming that the moment of inertia within the dogbone remains constant at a value equal to I_e. The M/EI diagram for this situation is qualitatively illustrated in Figure 3.3. The tip deflection was then calculated using the numerical integration, as described above. A value of I_e was determined so that the computed tip deflection was identical to the value computed using the exact moment of inertia.

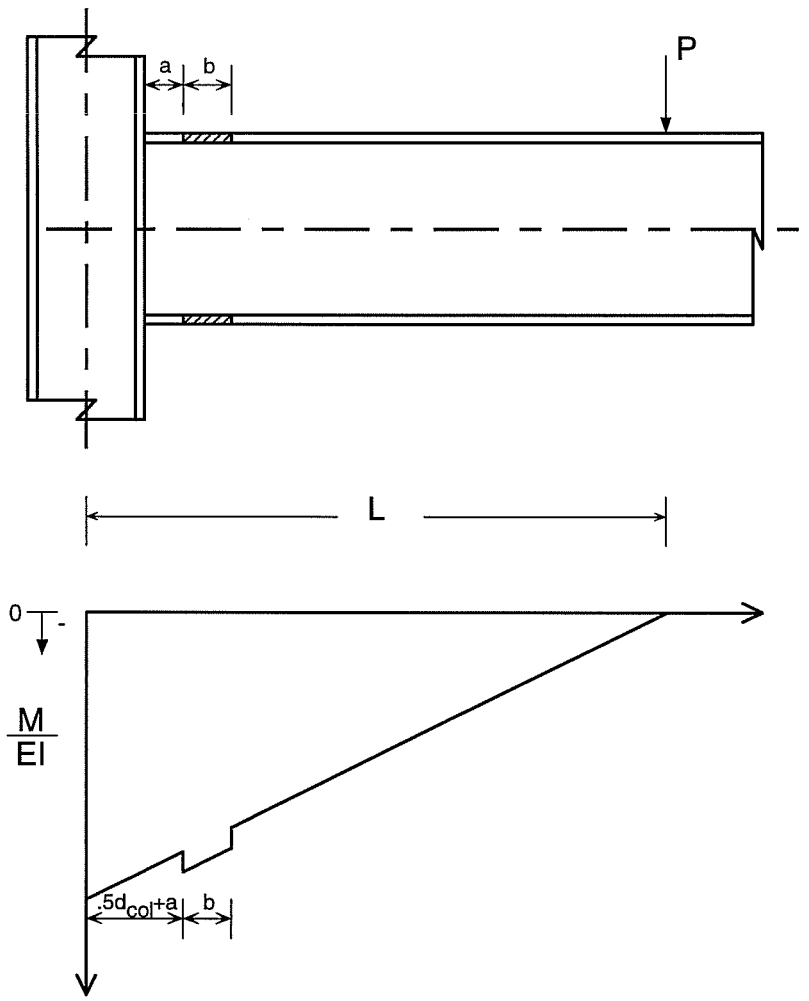

Figure 3.3: M/EI Diagram for Beam with I_e

By using this procedure, the effective moment of inertia was derived for several size beams with varying span lengths. The percentage of flange cutout and cutout length were varied to assess the effect on the effective moment of inertia. The results of these derivations are included in the next section.

Results

The three beam sizes, considered in Chapter 2, each with a 15 foot span and a 20 foot span were analyzed. The dimensions of the radius-cut dogbone, as shown previously in Table 2.1, were utilized. For each beam, the cutout is approximately 40 percent of the flange width. Table 3.1 contains the results of this derivation, where I is the original moment of inertia of the beam.

Table 3.1: Results for Dogbones with 40 Percent Cutouts

	I	I_e	I_e/I
W36X150			
15′ Span	8902.5	6964.67	0.782
20′ Span	8902.5	6963.9	0.782
W30X148			
15′ Span	6609.15	5153.07	0.780
20′ Span	6609.15	5150.52	0.779
W24X68			
15′ Span	1802.12	1408.58	0.782
20′ Span	1802.12	1407.98	0.781

By examining the beams with 40 percent cutouts, the ratio of the effective moment of inertia to the original moment of inertia appeared to be consistent across all beam sizes and span lengths. For a 40 percent cutout of the flange width, the ratio, I_e/I, was approximately 0.78 for all cases. In other words, the

effective moment of inertia was 78 percent of the original moment of inertia for all cases. The varying beam sizes and span length seemed to have no effect on the effective moment of inertia.

After establishing that the effective moment of inertia was essentially identical for all beam sizes and span lengths for the 40 percent cutout, the percentage of cutout of the flange width was modified. Table 3.2 shows the results of these modifications. The dimensions, a and b, were kept the same, but the cutout depth, c, was changed in order to obtain certain percentages of cutout. A range of 10-50 percent of the flange width was cutout and the effective moment of inertia was determined for each case. The ratio, I_e/I, is shown for each case.

Table 3.2: I_e/I for Various Cutouts

	10% Cutout	20% Cutout	30% Cutout	40% Cutout	50% Cutout
W36X150					
15′ Span	0.9471	0.8930	0.8373	0.7820	0.7204
20′ Span	0.9471	0.8929	0.8373	0.7820	0.7203
W30X148					
15′ Span	0.9482	0.8936	0.8260	0.7797	0.7076
20′ Span	0.9478	0.8932	0.8257	0.7793	0.7072
W24X68					
15′ Span	0.9471	0.8914	0.8340	0.7816	0.7134
20′ Span	0.9467	0.8911	0.8338	0.7813	0.7131

Reaffirming prior results, the effective moments of inertia remain nearly constant for all beam sizes and span lengths for the same percentage of flange width cutout. The ratios, I_e/I, were approximately 0.95, 0.89, 0.83, 0.78, and 0.71 for the 10, 20, 30, 40, and 50 percent cutouts, respectively. Also, the effective moment of inertia decreases as the percentage of cutout of the flange width increases.

The effect of the variation of the cutout length on I_e was also investigated. The length of the cutout, b, was increased by 50 percent. The percentage of cutout

was also varied. The ratios, I_e/I, after the increase in the cutout length are shown in Table 3.3.

Table 3.3: I_e/I for Various Cutouts - Dogbone Length Increased by 50 Percent

	10% Cutout	20% Cutout	30% Cutout	40% Cutout	50% Cutout
W36X150					
15′ Span	0.9475	0.8937	0.8386	0.7843	0.7232
20′ Span	0.9474	0.8936	0.8385	0.7840	0.7229
W30X148					
15′ Span	0.9486	0.8944	0.8275	0.7816	0.7104
20′ Span	0.9481	0.8939	0.8270	0.7811	0.7099
W24X68					
15′ Span	0.9477	0.8926	0.8361	0.7844	0.7176
20′ Span	0.9473	0.8922	0.8357	0.7840	0.7172

When comparing Table 3.2 and Table 3.3, the results are nearly identical. The increase in the cutout length had no significant effect on the effective moment of inertia. For the same cutout percentage, the ratio of effective moment of inertia to the original moment of inertia remains the same for different beam sizes and span lengths.

In summary, the results of these derivations are consistent and encouraging. The effective moment of inertia decreased with an increase in the amount cut out of the flange. For the same size cutout, the ratio of the effective moment of inertia to the original moment of inertia was nearly constant of regardless of the beam size, span length, or length of cutout. Table 3.4 contains an average I_e/I from all of the derivations.

Table 3.4: Summary of Results

	Average I_e/I
10% Cutout	0.948
20% Cutout	0.893
30% Cutout	0.833
40% Cutout	0.782
50% Cutout	0.715

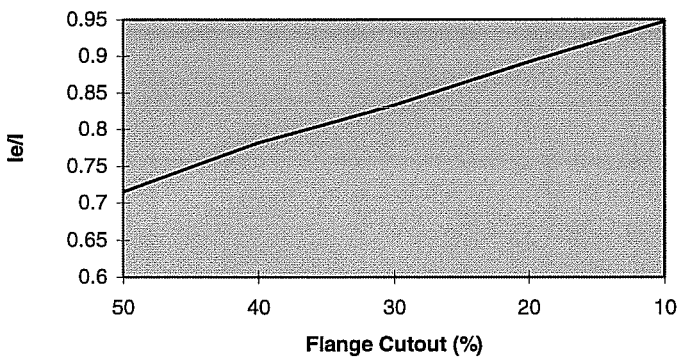

Figure 3.4: Plot of I_e/I vs. Flange Cutout

A plot of the results in Table 3.4 is shown in Figure 3.4. The relationship between the effective moment of inertia and the percent of the flange cutout was almost linear. With this graph, an effective moment of inertia can be approximated for any beam size, span length, or length of cutout. By performing linear regression for the data in Table 3.4, the following equation results for estimating I_e/I:

$$\frac{I_e}{I} = \frac{100 - 0.57[\%cutout]}{100} \tag{3.1}$$

For example, for a 30 percent cutout, Equation 3.1 gives I_e/I equal to 0.829.

An approximation of the effective moment of inertia can be useful when modeling a beam or a frame. With the depth of the cutout known, the effective moment of inertia can be computed from the information taken from Figure 3.4 or from Equation 3.1. As discussed earlier and shown in Figure 3.1, a separate member the length of the cutout can be created with this effective moment of

inertia. The frame analysis included in the next chapter used this modeling technique along with the results from this section in order to analyze the effects of the radius-cut dogbone connection on the stiffness of a frame.

Comparison with Finite Element Results

In order to evaluate the results from Table 3.4 and Equation 3.1, a cantilever beam was analyzed assuming the moment of inertia within the dogbone region remained constant at a value equal to I_e and the results compared to those from the finite element analysis. The cantilever beams were modeled in SAP90 with a separate member for the cutout region with 40 percent of the beam flange width removed. Table 3.5 includes the displacements in inches of the simplified analysis using frame elements and the finite element analysis.

Table 3.5: Comparison of Tip Displacements: Simplified Analysis Using Frame Elements vs. Finite Element Analysis

	Simplified Analysis Using Frame Elements (inches)	Finite Element Analysis (inches)
W36X150		
15′ Span	2.256	2.274
20′ Span	5.142	5.140
W30X148		
15′ Span	2.994	3.016
20′ Span	6.766	6.801
W24X68		
15′ Span	10.259	10.427
20′ Span	23.585	23.928

The difference between the simplified analysis using frame elements and the finite element analysis is small, less than 2 percent for all cases. The effective moments of inertia found from Table 3.5 or Equation 3.1 proved to be accurate and reliable. When modeling a beam or frame with the dogbone connection, the simplified analysis using frame elements is an accurate alternative to a finite element analysis and does not require an extensive effort, unlike a finite element analysis.

Chapter 4: Frame Analysis

In this chapter, a number of complete steel moment frames, both with and without dogbone cutouts in the beams, will be analyzed for their deflection response under lateral loading. A variety of frame sizes and configurations, as well as a variety of dogbone cutout sizes are examined. The frames are modeled on SAP90 using conventional frame elements. The dogbone regions of the beams are modeled using the effective moment of inertia derived in Chapter 3. The purpose of these analyses is to evaluate the effect of the dogbone cutouts on lateral frame stiffness for a wide range of conditions.

The Frame Models

Four frames were modeled using SAP90. These frames were from actual buildings affected by the Northridge Earthquake and were included in an investigation conducted by the SAC Joint Venture (December, 1995). The frames analyzed varied in story height and number of bays in order to cover a wide range of frames. Frame 1, as shown in Figure 4.1, was a one bay, seven story frame. Frame 2 was a three bay, four story frame and is shown in Figure 4.2. Frame 3 was a four bay, eighteen story frame and is shown in Figure 4.3. Lastly, Frame 4, shown in Figure 4.4, was a three bay, two story frame. The dimensions and member sizes for these frames are reported by SAC (December, 1995).

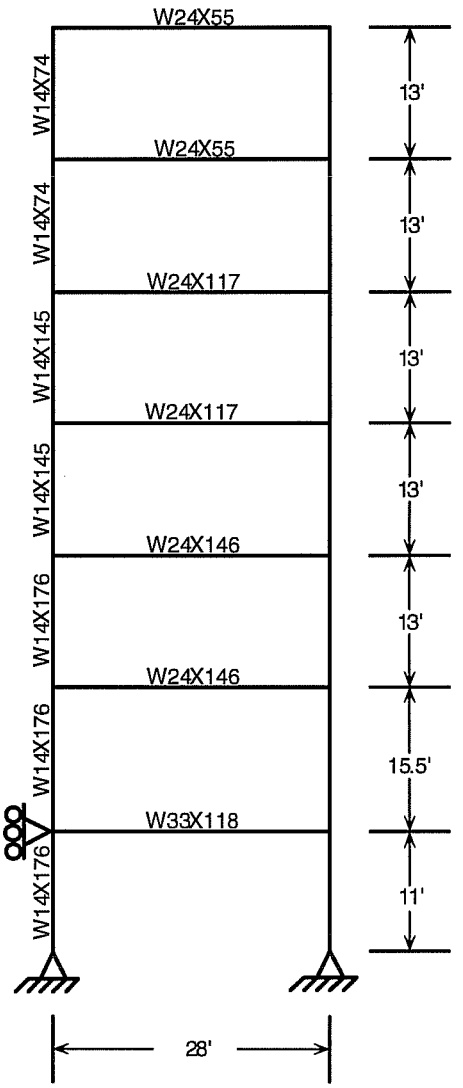

Figure 4.1: Frame 1

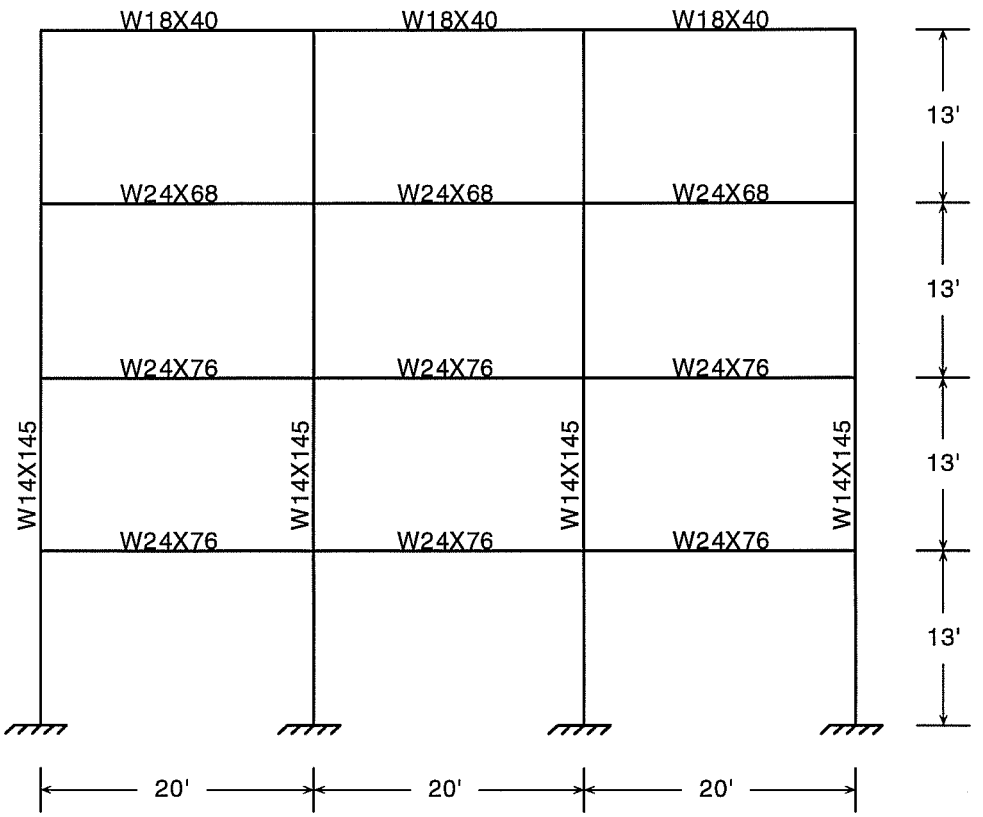

Figure 4.2: Frame 2

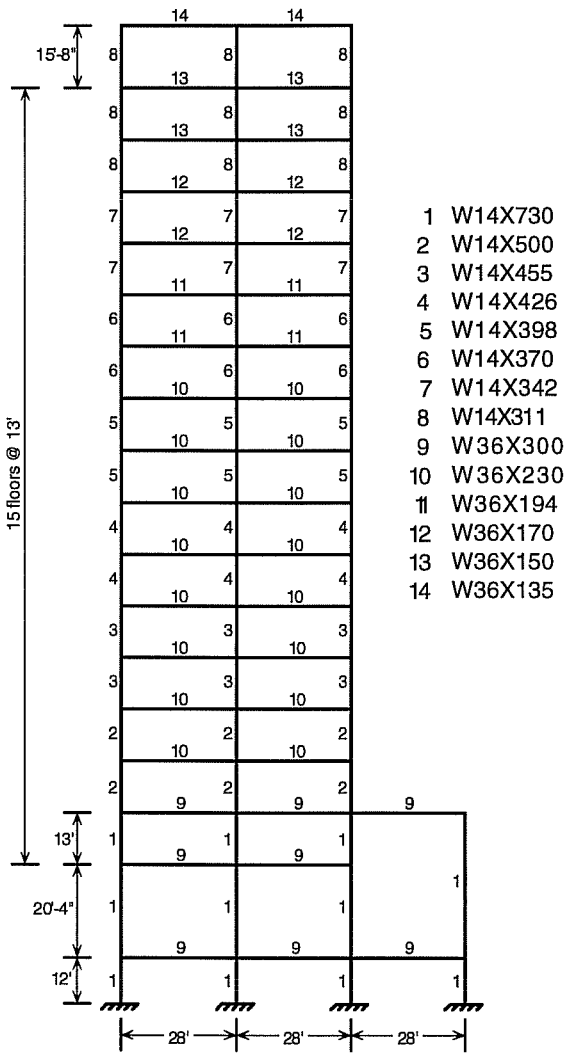

Figure 4.3: Frame 3

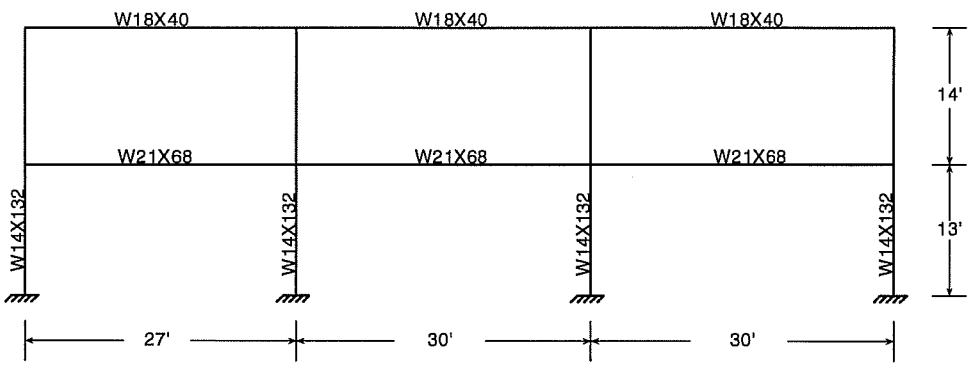

Figure 4.4: Frame 4

The frames were basically modeled by placing nodes at every joint. The beams were modeled similar to Figure 3.1. A separate member with the effective moment of inertia was included for the cutout region. The members of the frames not in the cutout region were taken from the AISC database of SAP90 where their section properties were automatically recovered.

Rigid end offsets were used at the beam-to-column connection to approximate the joint region. Rigid end offsets are the distances from the nodes to the faces of the supports, as shown in Figure 4.5. They are used because the dimensions of a structural member can be large enough to effect the stiffness of a frame. An analysis based upon centerline to centerline geometry, in general, overestimates the deflections. There are no member bending and shear deformations within the rigid offset lengths and all member forces are output at the outer ends of the rigid offsets or the face of the supports (Wilson & Habibullah, 1990). As recommended by the SAP90 User's Manual (Wilson & Habibullah, 1990), the length of the rigid zone was taken to be 50 percent of the actual joint dimension. This reduced length of the rigid zone accounts approximately for deformations within the joint region.

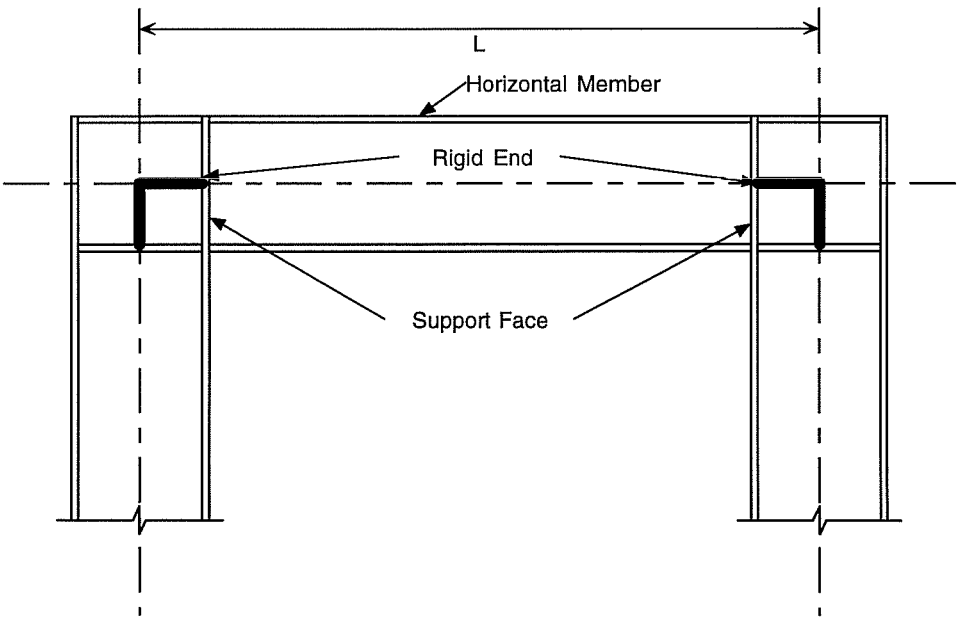

Figure 4.5: Rigid End Offsets (Wilson & Habibullah, 1990)

Following the guidelines established and previously discussed in Chapter 2, the key dimensions of the cutouts, shown in Figure 2.2, for each member size were determined. For each member, "a", the distance from the face of the column to the start of the dogbone, was taken as 75 percent of the flange width. The dimension "b", the length of the cutout, was configured at 85 percent of the beam depth. The cutout depth, "c", was varied. Each frame was analyzed with 10, 40, and 50 percent of the flange width cutout, where the percent cutout equals $2c/b_f$ times 100. For each beam size, Table 3.4 was used to calculate an effective moment of inertia for the corresponding percent cutout of the flange. As shown in Figure 4.6, the placement of the nodes in order to satisfy the dimensions of the cutouts and the rigid end offsets was crucial. One node was placed at the beam

and column centerlines. Another node was placed at a distance equal to half of the column depth plus "a" away from this node. From this node, another node was placed at a distance "b" away. The distance "b" is the length of the cutout and this member represents the cutout region. The cutout region has the calculated effective moment of inertia corresponding to the cutout percentage. In all cases, dogbone cutouts were added to both ends of all beams.

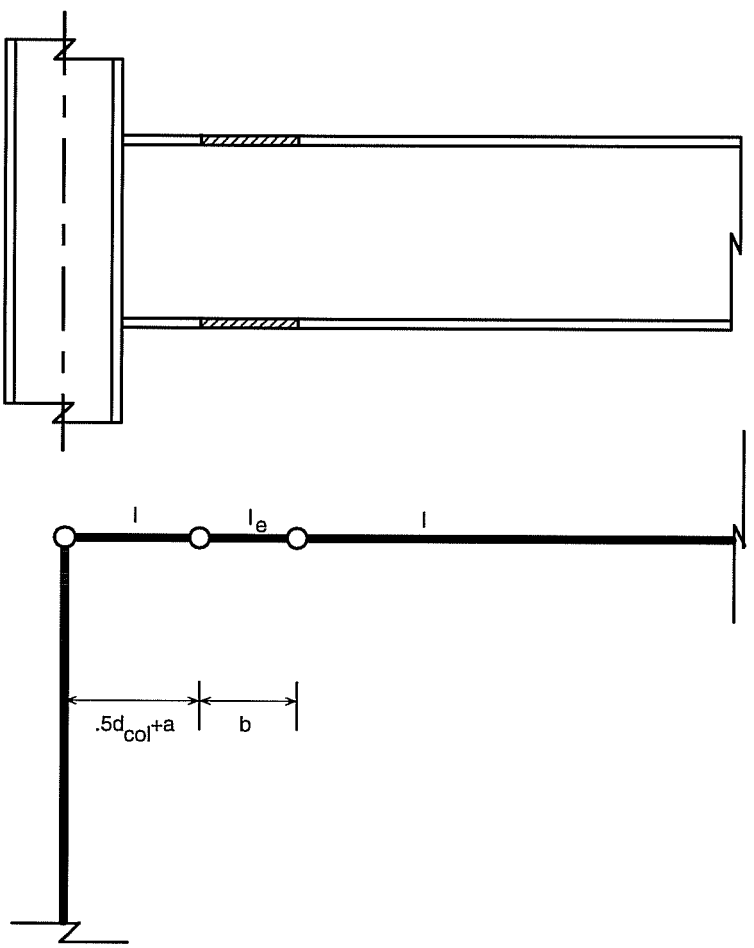

Figure 4.6: The Frame Model Dimensions

Results

Each frame was analyzed for two load cases: a constant lateral load of 10 kips and a triangular lateral load of 10 kips. As shown in Figure 4.7(a), for the constant load case, a concentrated load of 10 kips was placed laterally at each beam-to-column joint. For the triangular load case shown in Figure 4.7(b), a concentrated load of 10 kips was placed at the joint at the roof and then distributed triangularly along the story height. The total amount of load varied for each frame because of the different story heights. Since the change in stiffness caused by the dogbone cutouts is of interest here, the actual magnitude of the lateral load is irrelevant.

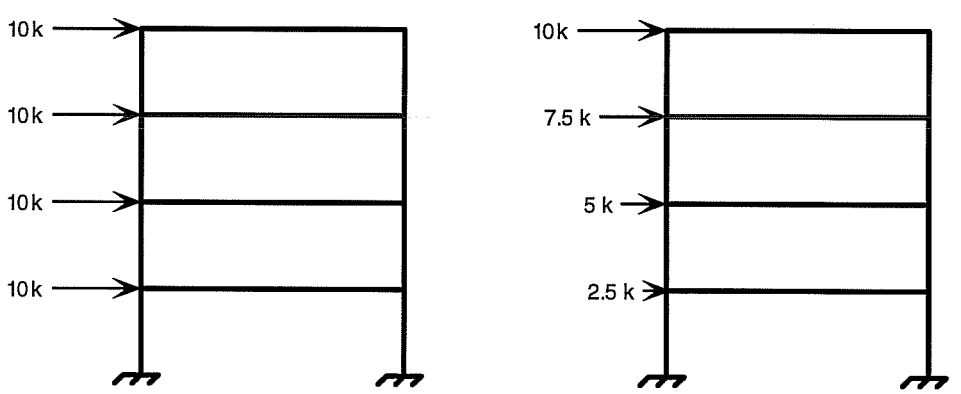

(a) Constant Lateral Load Case **(b) Triangular Lateral Load Case**

Figure 4.7: Two Loading Cases

As mentioned previously, building codes typically limit interstory drift, and therefore the examination of the maximum interstory drifts is crucial. The maximum interstory drift ratio and the roof displacement were examined for each frame. The interstory drift ratio was computed by taking the relative displacement for each story and dividing it by the story height. The maximum interstory drift ratio was found by comparing the interstory drift ratios of each story for a particular frame. The roof displacement was simply the total lateral displacement at the roof.

The results for Frame 1, Frame 2, Frame 3, and Frame 4 are shown in Table 4.1, Table 4.2, Table 4.3, and Table 4.4, respectively. The displacements are in inches and the maximum interstory drift is represented by a percentage.

Table 4.1: Results of Frame 1 Analysis

	Constant Loading	Triangular Loading
Roof Displacement		
Without Cutout	2.151 in.	1.644 in.
10% Cutout	2.169 in.	1.658 in.
40% Cutout	2.240 in.	1.713 in.
50% Cutout	2.276 in.	1.741 in.
Interstory Drift Ratio		
Without Cutout	0.250 %	0.200 %
10% Cutout	0.253 %	0.201 %
40% Cutout	0.261 %	0.208 %
50% Cutout	0.266 %	0.211 %

Table 4.2: Results of Frame 2 Analysis

	Constant Loading	Triangular Loading
Roof Displacement		
Without Cutout	0.387 in.	0.299 in.
10% Cutout	0.391 in.	0.302 in.
40% Cutout	0.405 in.	0.314 in.
50% Cutout	0.413 in.	0.320 in.
Interstory Drift Ratio		
Without Cutout	0.079 %	0.058 %
10% Cutout	0.080 %	0.059 %
40% Cutout	0.083 %	0.061 %
50% Cutout	0.084 %	0.062 %

Table 4.3: Results of Frame 3 Analysis

	Constant Loading	Triangular Loading
Roof Displacement		
Without Cutout	2.532 in.	1.818 in.
10% Cutout	2.556 in.	1.835 in.
40% Cutout	2.640 in.	1.896 in.
50% Cutout	2.683 in.	1.927 in.
Interstory Drift Ratio		
Without Cutout	0.121 %	0.080 %
10% Cutout	0.123 %	0.081 %
40% Cutout	0.127 %	0.084 %
50% Cutout	0.130 %	0.085 %

Table 4.4: Results of Frame 4 Analysis

	Constant Loading	Triangular Loading
Roof Displacement		
Without Cutout	0.161 in.	0.139 in.
10% Cutout	0.162 in.	0.140 in.
40% Cutout	0.167 in.	0.144 in.
50% Cutout	0.169 in.	0.146 in.
Interstory Drift Ratio		
Without Cutout	0.055 %	0.050 %
10% Cutout	0.055 %	0.050 %
40% Cutout	0.057 %	0.052 %
50% Cutout	0.058 %	0.052 %

The results shown in Tables 4.3 and 4.4 show that the roof displacements and the maximum interstory drift ratios increased as the percentage of flange cutout increased, as expected. The constant loading case displacements and interstory drift ratios were higher than the triangular loading case. This was expected because the triangular load had overall less lateral load than the constant loading.

By taking the roof displacements and the maximum interstory drifts, the change in stiffness of the overall frame was calculated for both those parameters. Tables 4.5, 4.6, 4.7, 4.8 include the percent change in stiffness based on roof displacements and on maximum interstory drift ratio for Frame 1, Frame 2, Frame 3, and Frame 4, respectively.

Table 4.5: Change in Stiffness Resulting From Dogbone - Frame 1

	Constant Loading	Triangular Loading
Change in Stiffness based on Roof Displacements		
10% Cutout	0.82 %	0.83 %
40% Cutout	4.10 %	4.16 %
50% Cutout	5.79 %	5.87 %
Change in Stiffness based on Max. Interstory Drift Ratio		
10% Cutout	0.88 %	0.79 %
40% Cutout	4.42 %	3.97 %
50% Cutout	6.24 %	5.61 %

Table 4.6: Change in Stiffness Resulting From Dogbone - Frame 2

	Constant Loading	Triangular Loading
Change in Stiffness based on Roof Displacements		
10% Cutout	0.94 %	0.97 %
40% Cutout	4.72 %	4.87 %
50% Cutout	6.66 %	6.69 %
Change in Stiffness based on Max. Interstory Drift Ratio		
10% Cutout	0.96 %	0.97 %
40% Cutout	4.80 %	4.84 %
50% Cutout	6.77 %	6.83 %

Table 4.7: Change in Stiffness Resulting From Dogbone - Frame 3

	Constant Loading	Triangular Loading
Change in Stiffness based on Roof Displacements		
10% Cutout	0.97 %	0.97 %
40% Cutout	4.29 %	4.29 %
50% Cutout	6.01 %	6.01 %
Change in Stiffness based on Max. Interstory Drift Ratio		
10% Cutout	1.26 %	1.24 %
40% Cutout	5.09 %	5.02 %
50% Cutout	7.06 %	6.96 %

Table 4.8: Change in Stiffness Resulting From Dogbone - Frame 4

	Constant Loading	Triangular Loading
Change in Stiffness based on Roof Displacements		
10% Cutout	0.68 %	0.70 %
40% Cutout	3.42 %	3.50 %
50% Cutout	4.81 %	4.92 %
Change in Stiffness based on Max. Interstory Drift Ratio		
10% Cutout	0.82%	0.81 %
40% Cutout	4.11 %	4.05 %
50% Cutout	5.79 %	5.70 %

For the same size cutout, the reduction in stiffness across all frame types and loading cases was very similar based upon the roof displacements or the maximum interstory drift ratios. When 10 percent of the flange width was cutout, the reduction in stiffness was approximately 1 percent for Frame 1, 2, 3, and 4 for both loading cases. The reduction in stiffness ranged from 4 to 5 percent for the standard size cutout of 40 percent. Finally, for the largest cutout of 50 percent, the reduction in stiffness of the overall frame was 5 to 7 percent.

Overall, these results indicate that the reduction in lateral frame stiffness resulting from the addition of dogbone cutouts in the beams is generally quite small. From a design perspective, this reduction in stiffness could be dealt with in several different ways. One option for a designer is to explicitly model the dogbone regions through the addition of separate frame elements, as was done in this chapter. By using the effective moment of inertia derived in Chapter 3 for the dogbone frame elements, the reduction in lateral stiffness of the frame due to the dogbones will be accurately predicted in the computer analysis of the frame. While this approach provides accurate results, it requires increased modeling effort. An alternative approach to avoid explicitly modeling the dogbone regions would be to run a conventional frame analysis without the dogbones, and simply adjust the results based on the data generated in this chapter. For example, if dogbones are used with 40 percent flange removal, the results of this study suggest that on average, interstory drift ratios increase approximately 4 percent over a broad range of frame configurations and heights. Thus, the interstory drifts predicted by a frame analysis without modeling of the dogbones could then simply be increased by 4 percent. While this approach is not as accurate, it

simplifies the computer modeling effort, and probably results in sufficient accuracy for design purposes. As a final option, a designer may consider the reduction in stiffness due to the dogbones to be negligible, and simply ignore this effect in the frame analysis and design. This, of course, is a matter of engineering judgment.

Chapter 5: Summary and Design Recommendations

Summary

The radius-cut dogbone connection has received considerable attention recently as an alternative for seismic-resistant steel moment frame connections. The dogbone connection has shown promising performance in previous research and testing in the areas of ductility and strength. It also appears to be an economical alternative based on recent cost studies. An area which has not been adequately investigated, however, is the reduction in elastic lateral frame stiffness caused by the use of the dogbone connection. The investigation of the frame lateral stiffness is important because code mandated drift limitations normally control the beam sizes. The reduction in stiffness of the frame due to the dogbone connection could increase the member sizes needed in a frame. In this report, the evaluation of the elastic lateral stiffness of steel moment frames with dogbone connections was completed in three steps: finite element analysis of cantilever beams, simplified analysis using frame elements, and a series of complete frame analyses.

The finite element modeling examined three different size individual cantilever beams with differing span lengths in order to determine the effect of the dogbone connection on the stiffness. With a 40 percent cutout of the flange width, the individual cantilever models showed a slight reduction in stiffness with the dogbone connection. The longer span showed a lower reduction in stiffness than the shorter span. The reduction in stiffness of the individual cantilever

beams ranged from 5 to 9 percent across all beam sizes and span lengths. The results of the finite element analysis were verified by a simplified closed form solution.

Since a finite element analysis of a beam with a dogbone cutout requires extensive effort, a simplified approach was developed in order to analyze a beam or a frame. The approach allows the dogbone region to be modeled as a single prismatic frame element with an effective moment of inertia, I_e. The effective moment of inertia was found as a percentage of the original moment of inertia of the beam. This permits calculating effective moments of inertia for any size beam. It was concluded that the cutout length and the span length has virtually no effect on the effective moment of inertia. As the cutout depth was increased, the effective moment of inertia decreased. For a 10, 20, 30, 40, and 50 percent cutout of the flange width, the ratio of the effective moment of inertia to the original moment of inertia was 0.95, 0.89, 0.83, 0.78, and 0.72, respectively. An equation was developed in order to compute the effective moment of inertia for any cutout size. In order to evaluate the simplified approach using frame elements, the results of this approach were compared to the finite element analysis results. The simplified approach using frame elements is quicker, less tedious, and more practical for design office use than the finite element analysis, but still provides reliable and accurate results.

In order to investigate the effect of the dogbone connection on the overall frame stiffness, a series of frame analyses were performed on several moment frames of varying heights and configurations. These analyses used frame elements with a reduced I_e to model the dogbone region of the beams. The roof

displacement and maximum interstory drift ratio was evaluated for different frame types with different sizes of dogbone cutouts in the beams. For a small 10 percent cutout of the flange width, the stiffness of the entire frame was reduced by about 1 percent. By using the standard cutout of 40 percent, there was a 4 to 5 percent reduction in stiffness for all frame types. Finally, for the largest cutout of 50 percent, the reduction in stiffness was from 5 to 7 percent.

Design Recommendations

After examining and analyzing the radius-cut dogbone connection, a small, but apparent, reduction in the elastic lateral stiffness of the overall frame resulted. The question is whether this reduction can be ignored or must be considered in the design. Basically, this is a matter of engineering judgment. If one feels that the reduction is small enough to be negligible, the conclusion would be to ignore the effects of the dogbone connection on the elastic drift calculations. Another option would be to take into account the small stiffness change by adjusting computed drift after a frame analysis without dogbone connections is completed. Finally, the last option is to design the frame taking into account the reduction in stiffness caused by the dogbone connection by modeling the dogbone regions with additional frame elements. A structural analysis program would accurately predict the reduction in lateral stiffness.

Bibliography

Chen, S.J. and Yeh, C.H., "Enhancement of Ductility of Steel Beam-to-Column Connections for Seismic Resistance," presented at the 1994 SSRC Task Group Meeting and Technical Session.

Engelhardt, M., Winneberger, T., Zekany, A., and Potyraj, T., "The Dogbone Connection Part II," *Modern Steel Construction*, Vol. 36, No. 8, American Institute of Steel Construction, August, 1996.

Horne, M.R. and Morris, L.J. *Plastic Design of Low-rise Frames*. Great Britain: Granada Publishing Limited, 1981, pp. 2-3.

Iwankiw, N.R., and Carter, C.J., "The Dogbone: A New Idea to Chew On," *Modern Steel Construction*, Vol. 36, No. 4, American Institute of Steel Construction, April, 1996.

Kassamali, Aslam. *Structural Analysis*. Boston: PWS Publishing Company, 1993, pp. 200-210.

Load and Resistance Factor Design, Volume 1, Second Edition, Manual of Steel Construction, American Institute of Steel Construction.

Plumier, A., "New Idea for Safe Structures in Seismic Zones," *IASE Symposium*, Brussels, 1990.

Popov, E.P., "UCB Specimen DB1," Test Summary Memo, University of California at Berkeley, February, 1996.

SAC Joint Venture, "Interim Guidelines: Evaluation, Repair, Modification and Design of Steel Moment Frames," *Report No. SAC-95-02*, Federal Emergency Management Agency, August, 1995.

SAC Joint Venture, "Technical Report: Analytical and Field Investigations of Buildings Affected by the Northridge Earthquake of January 17, 1994," *Report No. SAC 95-04*, Parts 1 & 2, Federal Emergency Management Agency, December, 1995.

Timoshenko, S. and Gere, J. *Mechanics of Materials.* New York, N.Y.: Van Nostrand Reinhold Company, 1972, p. 202.

Tremblay, R., Tchebotarev, N. and Filiatrault, A., "Seismic Performance of RBS Connections for Steel Moment Resisting Frames: Influence of Loading Rate and Floor Slab," *Proceedings; STESSA '97*, Kyoto, Japan, August 4-7, 1997.

Wilson, E., and Habibullah, A., *SAP90 Users Manual*, Computers & Structures, Inc., University of California at Berkeley, 1989.

Vita

Kristin Victoria Grubbs was born in Baltimore, Maryland, on June 4, 1973, the daughter of Steven Arthur Grubbs and Connie Pitts Grubbs. After completing her work at L.D. Bell High School, Hurst, Texas, in 1991, she entered Texas A&M University in College Station, Texas. During her undergraduate studies, she interned for EMCON Baker-Shiflett, Inc. of Fort Worth, Texas, and for Wiss, Janney, Elstner Associates, Inc. of Irving, Texas. She received the degree of Bachelor of Science in Civil Engineering from Texas A&M University in December, 1995. After graduating, she enrolled at The University of Texas at Austin in January, 1996, to pursue graduate studies in Structural Engineering where she was a Teaching Assistant for a materials class.

Permanent address: 1105 Clear View Drive
Bedford, Texas 76021

This thesis was typed by the author.